DIFFRACTIVE HARD INTERACTIONS IN ELECTRON PROTON COLLISIONS

J. P. Phillips

Department of Physics, University of Liverpool, England

A new analysis of diffractive deep-inelastic ep scattering at HERA is presented using data taken in 1994 with the H1 detector corresponding to an integrated luminosity of $\sim 2\,\mathrm{pb}^{-1}$. The cross section is measured in terms of a diffractive structure function $F_2^{D(3)}(\beta, Q^2, x_{I\!P})$ of the proton over the kinematic range $2.5 < Q^2 < 65$ GeV^2, $0.01 < \beta < 0.9$ and $0.0001 < x_{I\!P} < 0.05$. The dependence of $F_2^{D(3)}$ on $x_{I\!P}$ is found not to depend on Q^2 but to depend on β, demonstrating that the factorisation of the $\gamma^* p$ cross section into a universal diffractive flux (depending only on $x_{I\!P}$) and a single structure function (depending only on β and Q^2) is not tenable. The data are consistent with an interpretation in which two individually factorisable components contribute to $F_2^{D(3)}$. They may be identified with pomeron ($I\!P$) and meson Regge trajectories with $x_{I\!P}$ dependencies $\propto x_{I\!P}^{-n_{I\!P}}$, $x_{I\!P}^{-n_M}$ where $n_{I\!P} = 1.29 \pm 0.03(\mathrm{stat}) \pm 0.07(\mathrm{syst})$ and $n_M = 0.3 \pm 0.3(\mathrm{stat}) \pm 0.6(\mathrm{syst})$. The Q^2 and β dependences of $F_2^{D(3)}$ are examined in the form of $\tilde{F}_2^D(\beta, Q^2)$ after integrating over the dependence on $x_{I\!P}$. For different β, violations of scale invariance are observed which are consistent with a substantial gluon component in diffractive exchange. When confronted with the leading order DGLAP evolution equations in perturbative QCD, the data yield first estimates of the partonic content of diffractive exchange. Measurements are presented of energy flow, inclusive charged particle spectra and inclusive charm production in diffractive interactions at high Q^2, and of diffractive di–jet production at both $Q^2 = 0$ and $Q^2 \gg 0$. These characteristics of the final state are consistent with calculations based on a partonic model of e-$I\!P$ interactions in which the parton distributions are taken from the QCD analysis of $F_2^{D(3)}$.

1 Introduction

Deep–inelastic electron–proton (ep) scattering (DIS) has long been anticipated as an excellent opportunity to study the short distance structure of diffractive interactions[1,2,3]. High Q^2 ep interactions in which the incident proton interacts with low energy and momentum transfer make possible measurements of the short distance structure of the diffractive exchange ($I\!P$) in a similar way to that in which the partonic structure of the proton may be studied in inclusive DIS[4]. The data taken in 1992 at HERA led to the first observation of DIS events with an interval of rapidity around the incident proton direction devoid of hadron production - a "rapidity gap"[5,6]. The 1993 data from HERA provided first measurements of the contribution of such events to the DIS cross section, quantified in terms of a structure function $F_2^{D(3)}$[7,8], which demonstrated that the production mechanism is dominantly diffractive, and that the substructure of diffractive exchange is of a point–like, and presumably partonic, nature. First indications of a large gluonic contribution to this partonic substructure at high Q^2 were obtained[9,10]. Considerably more precise 1994 preliminary H1 results on diffractive hard interactions are presented here.

2 The Cross Section for Diffractive Deep–Inelastic Scattering

In order to measure an experimentally well defined cross-section for diffractive DIS the measurement is defined in terms of the diagram shown in figure 1. The hadronic final state in any event may

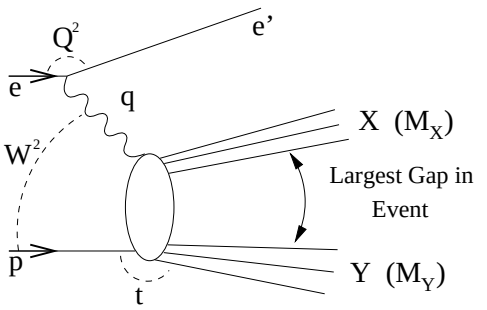

Figure 1: Schematic definition of the systems X and Y, which are separated by the largest gap in the distribution of rapidity defined with respect to the $\gamma^* p$ axis.

be decomposed into two systems, X and Y, that are separated by the largest gap in the rapidity distribution of the final state (excluding the scattered lepton), where rapidity is defined with respect to the $\gamma^* p$ axis. A cross-section is then measured at different values of the invariant masses, M_X and

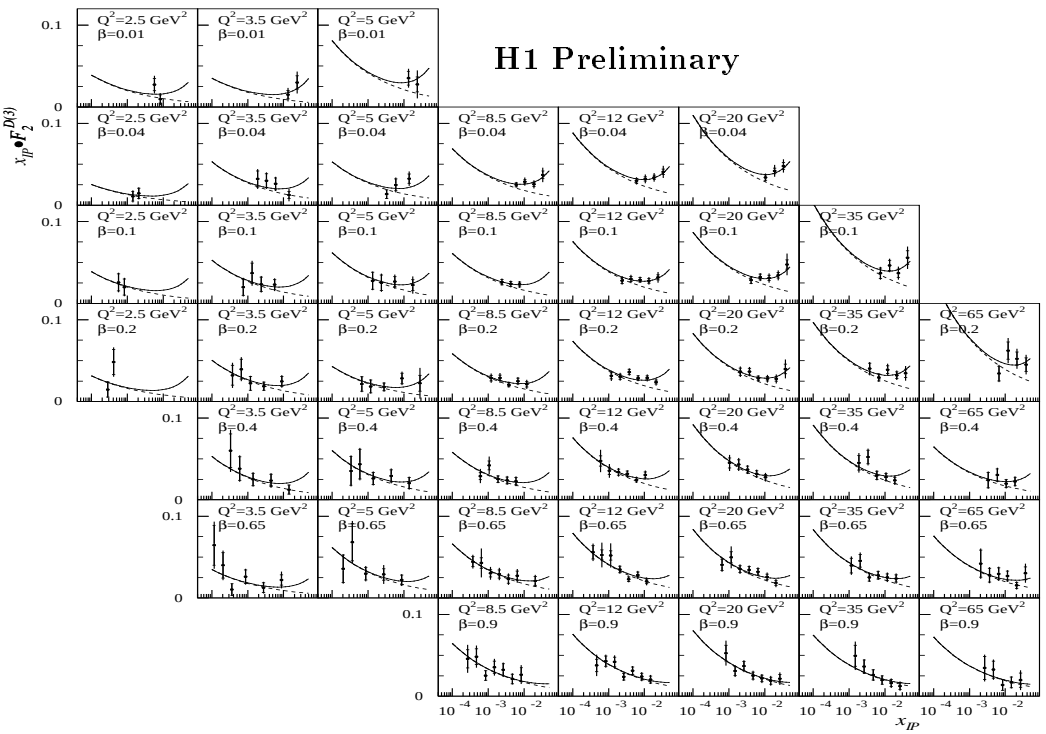

Figure 2: $x_{I\!P} \cdot F_2^{D(3)}(\beta, Q^2, x_{I\!P})$ as a function of $x_{I\!P}$ for different values of β and Q^2. Also shown is the result of a phenomenological fit in which two separately factorisable (non-interfering) components contribute to the measured cross section. The dashed line is the pomeron component and the solid line the total.

M_Y, of the two systems, interpretable as "diffractive" when both masses are small in comparison with the centre of mass energy W. Under such circumstances, a large rapidity gap must always occur from kinematic considerations alone.

Defining $Q^2 = -q^2$ and $W^2 = (q+P)^2$ in the usual way, where q and P denote the 4-vectors of the virtual photon and the proton respectively, further kinematic variables are defined as

$$t = (P-Y)^2, \quad x_{I\!P} = \frac{Q^2 + M_X^2}{Q^2 + W^2}, \quad \beta = \frac{Q^2}{Q^2 + M_X^2}.$$

β is then the Bjorken-x variable for scattering off the exchanged system with 4-momentum $(P-Y)$.

The experimental selection of events is based on an absence of hadron production in regions of the H1 detector covering a laboratory pseudorapidity interval $3.4 < \eta < 7.5$ [a]. The system X is then taken to be composed of all particles produced backward of this gap. The lower limit of 7.5 on the pseudorapidity reached by particles in the leading system, Y, restricts its mass to $M_Y < 1.6$ GeV and the squared 4-momentum transfer $|t|$ to be less than $\sim 1.6\,\mathrm{GeV}^2$.

The data are used to measure a cross-section for the process, $ep \to e'XY$, differential in $x_{I\!P}$, β and Q^2, in the kinematic range $2.5 < Q^2 < 65\ \mathrm{GeV}^2$, $0.01 < \beta < 0.9$ and $0.0001 < x_{I\!P} < 0.05$, integrated over the region $M_Y < 1.6$ GeV and $|t| < 1\ \mathrm{GeV}^2$. Following the procedure proposed in [2], the results are presented in terms of a diffractive structure function $F_2^{D(3)}(\beta, Q^2, x_{I\!P})$ which is related to the differential $ep \to e'XY$ cross section by

$$\frac{\mathrm{d}^3\sigma^D_{ep\to eXY}}{\mathrm{d}x_{I\!P}\,\mathrm{d}\beta\,\mathrm{d}Q^2} = \frac{4\pi\alpha^2}{\beta Q^4}\left(1 - y + \frac{y^2}{2}\right) F_2^{D(3)}(\beta, Q^2, x_{I\!P}).$$

The quantity, $x_{I\!P} \cdot F_2^{D(3)}(\beta, Q^2, x_{I\!P})$ is shown as a function of $x_{I\!P}$ in figure 2 for different values of β and Q^2. In a Regge interpretation [11], in which the $x_{I\!P}$ dependence is assumed to describe

[a] The H1 coordinate system is defined such that positive rapidity corresponds to the proton beam direction.

a reggeon flux associated with the proton, one expects a behaviour of the form $F_2^{D(3)} \propto 1/x_{I\!P}^n$ with $n \approx 2\alpha(0) - 1$, where $\alpha(t) = \alpha(0) + \alpha' t$ is the effective Regge trajectory. In practice, the finite values of t at which the measurement takes place are expected to reduce n relative to $2\alpha(0) - 1$ by a few percent.

The improved precision and extended kinematic range of these new data reveal clear deviations from the universal factorisation observed in our previous measurement [13]. The variation in the dependence on $x_{I\!P}$ through the kinematic range is clearly visible in figure 3a, which shows the results of fitting the data to the polynomial dependence $1/x_{I\!P}^n$ where n is allowed to vary with β but not with Q^2 ($\chi^2/ndf = 161/152$). In figure 3b the

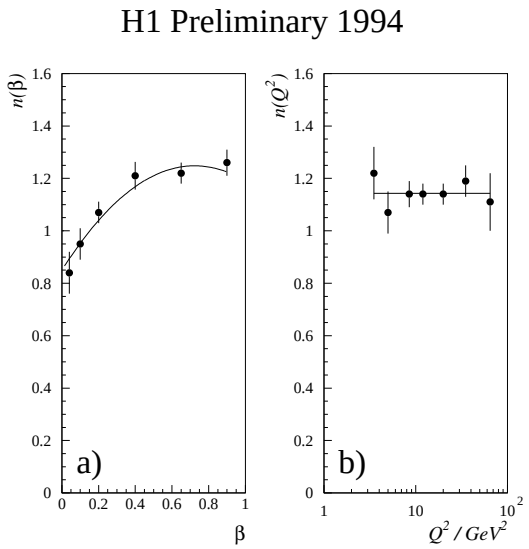

Figure 3: The results of a fit to the H1 data for $F_2^{D(3)}$ of the form $F_2^{D(3)} = A(\beta, Q^2) x_{I\!P}^{-n}$ where n is permitted to vary with β (a) or with Q^2 (b).

value of n is allowed to vary with Q^2 but not β. There is no evidence for any dependence of n on $\ln Q^2$, and the resulting β averaged value of n is entirely consistent with our previous measurement [13] for each value of Q^2.

One possible explanation for the decrease in n for $\beta \lesssim 0.2$ to values below unity is that there is a contribution to the measured cross section from sub-leading trajectories which may be identified with the exchange of quantum numbers corresponding to physical meson states. After the pomeron, the next–leading exchanges are the approximately degenerate trajectories with the quantum numbers of the ρ, ω a_2 and f_2 mesons, for which one would expect $n \sim 0$ or less, and which may have a much softer β dependence than that of the leading vacuum trajectory.

Superimposed on the data in figure 2 is the result of a fit to the data in which both a pomeron component $F_2^{I\!P}(\beta, Q^2) \cdot x_{I\!P}^{-n_{I\!P}}$ and meson component $C_M \cdot F_2^M(\beta, Q^2) \cdot x_{I\!P}^{-n_M}$ contribute to $F_2^{D(3)}$. Here, the meson and pomeron terms are assumed not to interfere. The parameters C_M, $n_{I\!P}$ and n_M are free parameters in the fit along with the value of $F_2^{I\!P}(\beta, Q^2)$ at each separate value of β and Q^2. Since no measurements of the structure function of such mesons exist, the function $F_2^M(\beta, Q^2)$ is taken from a GRV parameterisation of the pion structure function [14]. The systematic effect on the values of the parameters extracted from the fit procedure is found to be small for any for any choice of $F_2^M(\beta, Q^2)$ which falls with increasing β (see [12] for details).

Figure 4 highlights the data for $x_{I\!P} \cdot F_2^{D(3)}(\beta, Q^2, x_{I\!P})$ at $Q^2 = 20\,\mathrm{GeV}^2$ for $\beta = 0.1$ and $\beta = 0.9$. Also shown is a fit to the data, which is

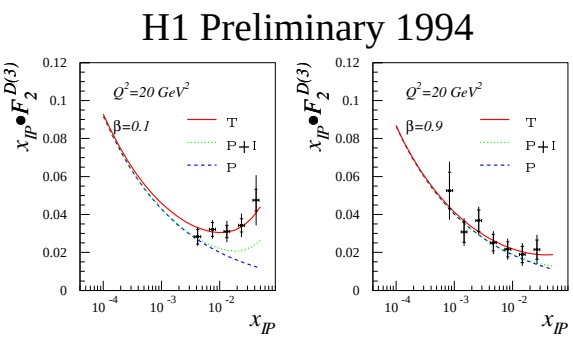

Figure 4: $x_{I\!P} \cdot F_2^{D(3)}(\beta, Q^2, x_{I\!P})$ as a function of $x_{I\!P}$ for $Q^2 = 20\,\mathrm{GeV}^2$ for a) $\beta = 0.1$ and b) $\beta = 0.9$. Also shown is the result of a phenomenological fit in which pomeron and meson components interfere with a relative phase of 45°. The pomeron (P) component, pomeron + interference (P+I) components and total (T) are displayed separately.

identical to that above except that the pomeron and meson amplitudes interfere with a relative phase of 45° (neglecting the t dependence of the phase and corresponding to the case in which the only sub-leading trajectory which contributes is the f_2.) It is evident that the soft β distribution assumed for the meson structure function results in a contribution to $F_2^{D(3)}(\beta, Q^2, x_{I\!P})$ that is

predominantly at very low β. The introduction of interference in this fit results in a large reduction in the magnitude of the pure meson intensity. However, the fitted intercepts of the pomeron and meson trajectories, along with the normalisation of the pure pomeron intensity, remain largely unchanged from those obtained in the fit without interference.

A good description of the data is obtained for both fits (χ^2/ndf = 165/156 and 170/156 respectively), and correcting [b] for the integration over t yields $\alpha_{I\!P}(0) = 1.18 \pm 0.02(\text{stat}) \pm 0.04(\text{syst})$ and $\alpha_M(0) = 0.6 \pm 0.1(\text{stat}) \pm 0.3(\text{syst})$ for the intercepts of the pomeron and meson trajectories respectively. Here the systematic errors include those associated with the treatment of the meson structure function and the inclusion or exclusion of interference. The value of α_M is entirely consistent with that expected for the sub-leading trajectory. The value of $\alpha_{I\!P}(0)$ is somewhat larger than that obtained in some parameterisations of soft hadronic interactions [15].

3 Forward Neutron Production

Contributions to the measured cross section from processes involving the exchange of charged mesons may be quantified by tagging highly energetic forward neutrons in the H1 leading neutron calorimeter. The uncorrected energy spectrum for such neutrons in DIS events (without any diffractive selection) is shown in figure 5. At large neutron energy the data are well reproduced by a model of charge exchange based upon π^+ exchange [16,17]. It estimated that $3.3^{+3.0}_{-1.0}$% of events in the kinematic region $x_{I\!P} < 0.05$ (the region in which the $F_2^{D(3)}$ measurements is made) have a leading neutron. This small fraction of events is insufficient to explain the observed deviations from universal factorisation. If proton dissociation is assumed to be the only mechanism producing energetic neutrons for $x_{I\!P} < 0.05$ then the fraction of proton dissociation in this kinematic range is estimated to be 25^{+32}_{-9}%.

[b] Assumptions about the linearity and slope of both the pomeron and meson trajectories are necessary [12].

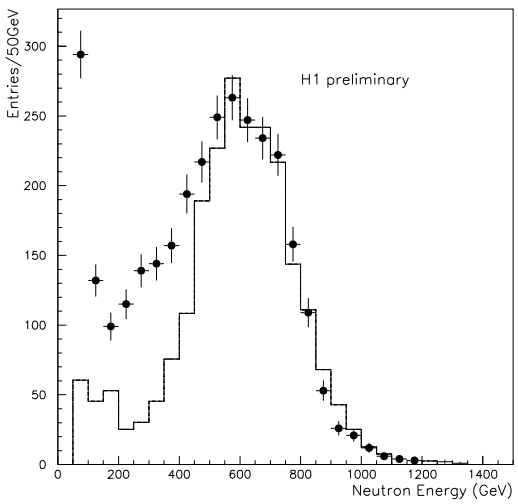

Figure 5: Uncorrected energy distribution of forward neutrons in DIS events. Also shown is the result of a Monte Carlo calculation based on π^+ exchange (see text).

4 QCD analysis

In the factorisable prescription proposed in [2], $\int \mathrm{d}x_{I\!P} F_2^{D(3)}(\beta, Q^2, x_{I\!P})$ describes the partonic structure of the diffractive exchange in an analogous way to $F_2(x, Q^2)$ in the case of the proton. Despite the observation of non-factorisation of the measured cross-section, performing the integration over $x_{I\!P}$ provides a measurement of the average deep-inelastic structure of whatever colourless exchanges contribute in the kinematic domain accessed.

We define

$$\tilde{F}_2^D(\beta, Q^2) = \int_{x_{I\!P}=0.0003}^{x_{I\!P}=0.05} F_2^{D(3)}(\beta, Q^2, x_{I\!P}) \mathrm{d}x_{I\!P}$$

which is proportional to the structure function for the exchange averaged over the range, $t_{min}(x_{I\!P}) \geq t > -1\,\mathrm{GeV}^2$ and $0.0003 \leq x_{I\!P} \leq 0.05$. Fig. 6 shows $\tilde{F}_2^D(\beta, Q^2)$ as a function of Q^2 for fixed β. The most striking feature is that a rise with $\ln Q^2$ persists to values of β far in excess of the point ($x \sim 0.15$) at which the structure of the nucleon becomes dominated by valence quarks rather than gluons, and $\mathrm{d}F_2(x, Q^2)/\mathrm{d}\ln Q^2$ correspondingly becomes negative. The nature of the scaling violations of $\tilde{F}_2^D(\beta, Q^2)$ are thus in qualitative accord with the hypothesis of a substantial gluon component in the structure of the diffractive exchange.

A QCD analysis of $\tilde{F}_2^D(\beta, Q^2)$ confirms this qualitative picture. A $u + d + s$ flavour singlet quark distribution and a gluon distribution are parameterised at a starting scale, $Q_0^2 = 2.5$ GeV^2, as

$$x_{i/\mathbb{P}} \cdot f_i(x_{i/\mathbb{P}}) = A_i \, x_{i/\mathbb{P}}^{B_i} \, (1 - x_{i/\mathbb{P}})^{C_i}$$

where $i = q, g$ and $x_{i/\mathbb{P}}$ is the fraction of the exchange momentum carried by the parton. These parton distributions are then evolved using DGLAP [18] evolution to $Q^2 > Q_0^2$, with the values of $A_{q,g}$, $B_{q,g}$ and $C_{q,g}$ as fit parameters (see [12] for details). Figure 6a shows the best fit

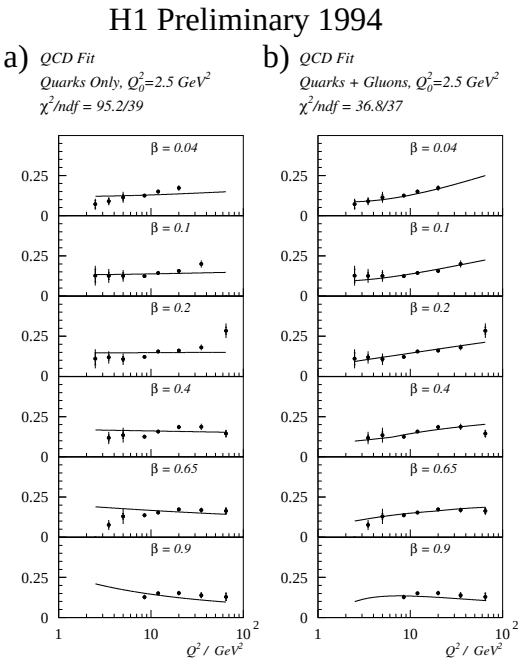

Figure 6: More completely random results.

obtained for $\tilde{F}_2^D$ when A_g is constrained to be zero, and only quarks contribute at the starting scale. Because of the persistence of rising $\ln Q^2$ scaling violations to high values of β, no such parameterisation is acceptable (confidence level CL = 0.00013%). An excellent (CL = 47.8%) fit, shown in figure 6b, can be obtained when gluons are also introduced at the starting scale. Excluding the data at $\beta = 0.9$, which correspond to the resonance region of $M_X \sim m_{\rho,\omega,\phi,\rho',\ldots}$ from the QCD analysis does not affect in any way the conclusions drawn.

5 Diffractive Final States

For a simple quark dominated pomeron the "struck" quark and the "remnant" will be aligned along the $\gamma^* I\!P$ axis, and so at the parton level, the only contributions to the transverse momentum arise from the intrinsic k_T of the quark and the remnant. The hadronisation process also contributes some transverse momentum. Both these contributions are expected to be relatively small ($\lesssim 1 GeV^2$). If the pomeron is a gluon dominated object, more transverse energy is produced. This arises as, in the boson-gluon fusion process (BGF), the quark anti-quark pair from the hard subprocess do not have to be aligned along the $\gamma^* I\!P$ axis since the quark propagator can have a finite virtuality.

Figure 7 shows the energy flow in the $\gamma^* I\!P$ centre of mass system as a function of pseudorapidity defined with respect to the $\gamma^* I\!P$ axis. The γ^* de-

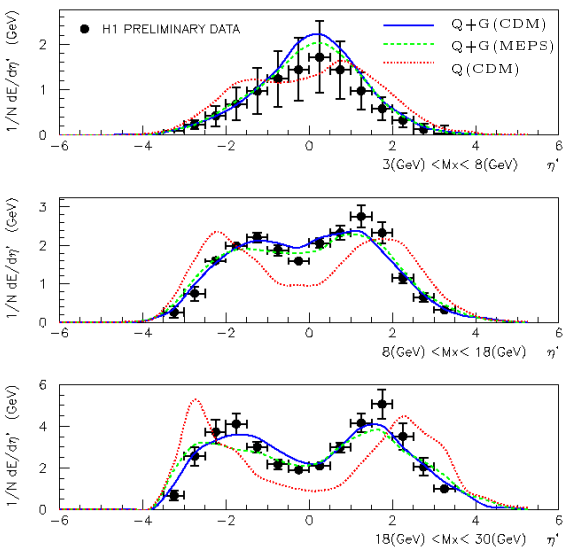

Figure 7: Energy flow as a function of η^* in the $\gamma^* I\!P$ frame at different values of M_X. The γ^* axis defines the positive z^* axis. Superimposed are the results of Monte Carlo calculations (see text).

fines the positive z^* axis, such that positive values of η^* correspond to the particle production associated with the fragmentation and hadronisation of the quark which couples to the virtual photon. The fully corrected H1 data are shown for three intervals of M_X between 3 and 30 GeV, and are compared to the predictions of Monte Carlo calculations, based upon a partonic model of $e I\!P$ colli-

sions[16,12]. Two sets of parton density function for the $I\!P$ are taken from the two solutions from QCD analysis described in section 4. The data exhibit a significant excess of energy production in the central region ($\eta^* \sim 0$) over the prediction of the "quark only" model Q(CDM), which undershoots the data at $\eta^* \sim 0$. The substantially increased relative abundance of boson–gluon fusion hard interactions in the "quark+gluon" model QG(CDM) results in an excellent description of the measured energy flow at all values of η^*, and this good description is unaffected by the adoption of an alternative fragmentation scheme, as in QG(MEPS)[12].

Boson–gluon fusion processes will result in an enhancement of high p_T^* single particle production. Figure 8a shows the distribution in p_T^* of charged charged tracks in the $\gamma^* I\!P$ centre of mass system. A significant excess at large values of p_T^* is

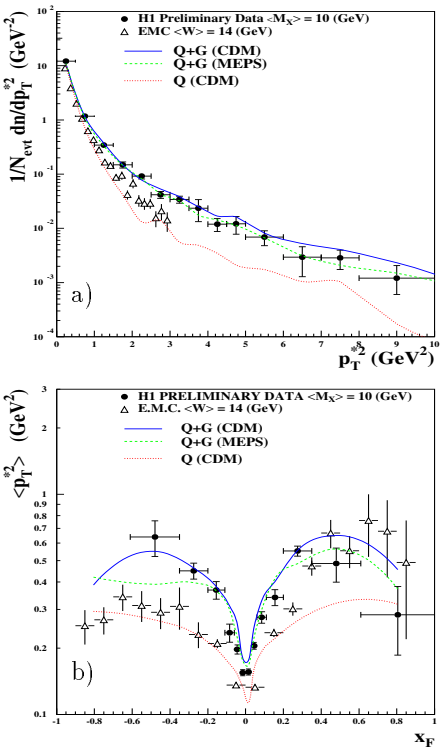

Figure 8: a) The p_T^* and b) $\langle p_T^* \rangle$ *vs* x_F for charged tracks in the $\gamma^* I\!P$ CMS system for H1 $\gamma^* I\!P$ data compared with EMC data in the $\gamma^* p$ CMS.

observed over the expectation of the quark dominated calculation, and this excess is reproduced well by both "leading gluon" calculations.

For ep diffractive interactions, the relevant mass scale for the hadronic final state is M_X. Therefore the H1 $\gamma^* I\!P$ data with $\langle M_X \rangle \sim 10$ GeV may be compared with inclusive $\gamma^* p$ data from the EMC experiment, also shown in figure 8a, which have a similar final state mean invariant mass $\langle W \rangle \sim 14$ GeV. The $\gamma^* p$ EMC data are strongly influenced by the valence and sea quark contributions to proton structure, and lie significantly below the H1 data at high p_T^*. Figure 8b shows a comparison of the H1 $\gamma^* I\!P$ data and the EMC $\gamma^* p$ data for the "seagull plot", in which the $< p_T^* >$ of charged tracks is shown as a function of Feynman-x, defined as $x_F = 2p_z^*/M_X$ for the H1 data and $x_F = 2p_z^*/W$ for the EMC data. The EMC data lie below the H1 data at all but the highest values of x_F, suggesting that a large proportion of the H1 diffractive events involve a high p_T hard subprocess. The $\gamma^* p$ EMC seagull plot is asymmetric, the average p_T in the remnant direction being lower than that observed in the struck parton direction. This can be attributed to the extended nature of the proton remnant, causing a reduction in the quantity of radiation in the remnant direction. In contrast, the H1 seagull plot is approximately symmetric about $x_F = 0$, suggesting that there is no suppression of gluon radiation in the backward hemisphere.

Figure 9a shows the cross section for the diffractive production of di–jets in the kinematic range $7.5 < Q^2 < 80\,\mathrm{GeV}^2$, $0.1 < y < 0.7$, $x_{I\!P} < 0.05$ and $P_T^{jet} > 5$ GeV. In leading order this di–jet cross section receives contributions from boson–gluon fusion and QCD–Compton diagrams, and so is highly sensitive to the partonic structure of the diffractive exchange. Since the measurement of $F_2^{D(3)}$ constrains tightly the sum of the quark distributions, and hence the QCD–Compton contribution to the di–jet cross section, then any large excess in the data over the prediction of the quark dominated Monte Carlo calculation Q(CDM) reflects the magnitude of the gluonic content of the exchange. The fractional momentum of the diffractive exchange carried by the di–jet system, $\xi_{I\!P}$, is reconstructed using the relationship $\xi_{I\!P} = \beta(1+M_{jj}^2/Q^2)$ where M_{jj} is the invariant mass of the di–jet system. For the Monte Carlo simulations use to correct the H1 data to the hadron level, this quantity has been established to be sensitive to the equivalent quantity at the

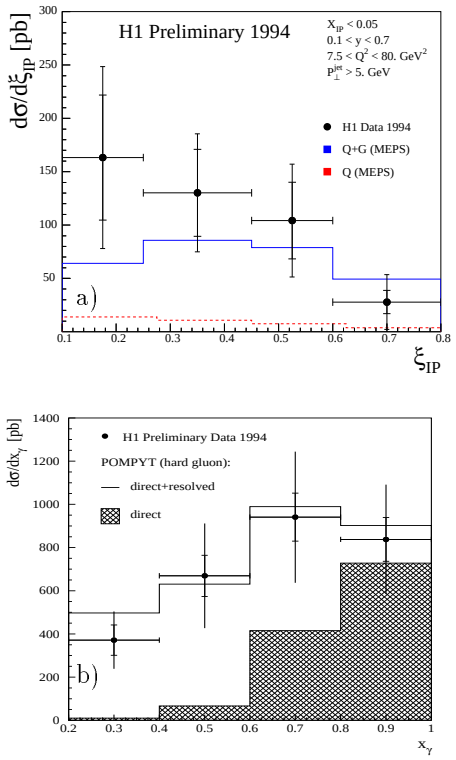

Figure 9: a) The cross section $d\sigma/d\xi_{I\!P}$ for the production of di-jets in diffractive DIS events. Also shown are two partonic Monte Carlo calculations which employ the parton distribution functions from the "quark+gluon" (upper histogram) and "quark" (lower histogram) QCD fits. b) The cross section $\mathrm{d}\sigma/\mathrm{d}x_\gamma^{OBS}$ for the photoproduction of di–jets. The POMPYT Monte Carlo calculation utilises a "hard" $z(1-z)$ gluon distribution, and is normalised to the data.

parton level $z = x_{i/I\!P}$, the fractional momentum of the diffractive exchange carried by the parton entering the hard interaction. The H1 data agree well in both shape and normalisation with the prediction of the "leading gluon" calculation, but are incompatible with the quark dominated calculation.

At $Q^2 = 0\,\mathrm{GeV}^2$ it is highly probable that diffractive di–jet production will receive contributions not only from processes in which the photon interacts as a whole (direct) but also from processes in which only a fraction of the photon momentum enters the hard scatter (resolved). Figure 9b shows the di–jet cross section[c] for the kinematic region $-1.5 < \eta_{jet} < 2.5$, $p_{T\,jet} > 5$ GeV, $x_{I\!P} < 0.05, 0.25 < y < 0.7$, and $10^{-8} < Q^2 < 0.01\,\mathrm{GeV}^2$. The cross section is plotted as a function of x_γ^{OBS}, the fractional momentum of the γ participating in the production of the di–jet system. x_γ^{OBS} is sensitive to the fractional momentum of the γ entering the hard interaction at the parton level. The cross section remains significant even at the lowest x_γ^{OBS}, in contrast to the expectation from a Monte Carlo calculation [19] containing only direct processes, indicating that resolved processes also contribute. A careful unfolding of the interplay between photon and pomeron structure is therefore a prerequisite to any further interpretation of the diffractive photoproduction di–jet cross section.

[c] The γp analysis is performed in the laboratory frame as for $Q^2 \sim 0\,\mathrm{GeV}^2$ the boost between this and the γp frame has no component transverse to the z axis.

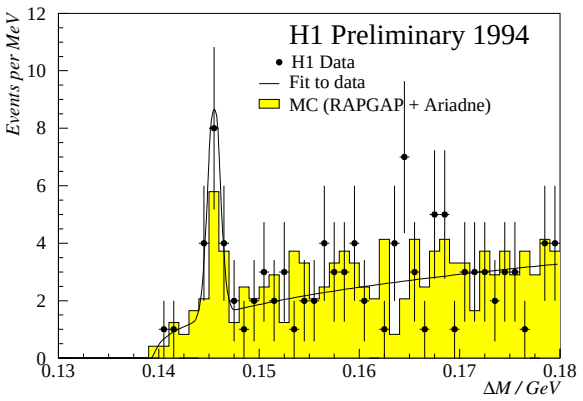

Figure 10: Distribution of the mass difference $\Delta M = M(K^-\pi^+\pi^+_{slow}) - M(K^-\pi^+)$. The shaded histogram shows the prediction of the Q+G(CDM) Monte Carlo which takes parton distribution functions from the "quark+gluon" QCD fit.

The large gluon distribution extracted from the QCD analysis described in section 4 should lead to a substantial cross section for diffractive open charm production through the boson–gluon fusion diagram $\gamma^* g \to c\bar{c}$. Such charm production has been searched for by looking for D^* production via the channel $D^{*\pm} \to D^0\pi^\pm_{slow} \to K^-\pi^+\pi^\pm_{slow}$. The first observation of $D^{*\pm}$ production in diffractive DIS interactions is shown in figure 10, and an ep cross section is measured in the kinematic range $10 < Q^2 < 100\,\mathrm{GeV}^2$, $0.06 < y < 0.6$, $x_{I\!P} < 0.05$, $M_Y < 1.6$ GeV, $|\eta(D^*)| < 1.25$ and $p_T(D^*) > 1$ GeV. The number of $D^{*\pm}$ candidates is found to be 11.6 ± 4*(stat)*, corresponding to an ep cross section of $380 \pm^{150}_{120\,stat} \pm^{140}_{110\,sys}$ pb. The "lead-

ing gluon" parton densities leads to a prediction of ~ 200 pb for this cross section, whilst the quark dominated solution of the QCD analysis predicts less than 10 pb [20].

6 Conclusions

A new measurement of the cross section for deep–inelastic diffractive ep scattering has been presented using data collected during 1994 from the H1 experiment at HERA.

With the improved precision and extended kinematic range of this new measurement, compared to our previous data [12], it is demonstrated that the factorisation from the cross section for diffractive DIS of a universal term describing a diffractive flux associated with the proton is no longer tenable. However, factorisation may be restored in an interpretation in which the leading trajectory, with intercept $\alpha_{I\!P}(0) = 1.18 \pm 0.02(\mathrm{stat}) \pm 0.04(\mathrm{syst})$, is accompanied by a sub–leading trajectory with intercept $\alpha_M(0) = 0.6 \pm 0.1(\mathrm{stat}) \pm 0.3(\mathrm{syst})$. This value of $\alpha_{I\!P}(0)$ is 2σ larger than the central values obtained in typical parameterisations of soft hadronic interactions [15].

The unambiguous observation of scaling violations in the Q^2 dependence of $\tilde{F}_2^D(\beta, Q^2)$ for fixed β in the form of a rising $\log Q^2$ dependence for $\beta \lesssim 0.65$ is interpreted in the framework of QCD in terms of a substantial contribution of gluons to the sub–structure of diffractive exchange. A DGLAP motivated QCD fit is found to require that the diffractive exchange evolves as if dominated by a leading gluon at the starting scale of $Q^2 = 2.5\,\mathrm{GeV}^2$. The application of the resulting parton distribution functions to a partonic model of $e I\!P$ interactions gives a consistent description of the topological features of energy flow, charged particle production, di–jet production, and charm production for the $Q^2 > 0$ data.

7 Acknowledgements

I would like thank my colleagues in H1 whose efforts made possible the results presented here. It is a pleasure to thank the organisers.

References

1. J. Ellis, "Discussion session on large Q^2 and hadron structure", Proceedings of the Study of an ep Facility for Europe, DESY **79-48**, April 2-3, 1979.
2. G. Ingelman and P. Schlein, Phys. Lett. **B152** (1985) 256.
3. H. Abramowicz, these proceedings.
4. For discussion see for example J. R. Forshaw and D. A. Ross, "QCD and the Pomeron", CUP, Cambridge, 1997.
5. ZEUS Collaboration, M.Derrick et. al. Phys. Lett. **B315** (1993) 481.
6. H1 Collaboration, T. Ahmed et. al. Nucl. Phys. **B429** (1994) 477.
7. H1 Collaboration, T. Ahmed et. al. Phys. Lett. **B348** (1995) 681.
8. ZEUS Collaboration, M. Derrick et. al. Z. Phys **C68** (1995) 569.
9. J. P. Phillips, "Rapidity Gap Events at HERA and the Structure of the Pomeron", in Proc. of the International Workshop on Deep–Inelastic Scattering and Related Topics, Paris, France, April 1995, p.359.
10. J. B. Dainton, "Deep–Inelastic Physics with H1 at the HERA ep Collider", in Proc. of the International Workshop on Deep–Inelastic Scattering and Related Topics, Paris, France, April 1995, p.37;
    J. B. Dainton, "Deep–Inelastic Electron-Proton Diffraction", DESY **95-228**.
11. See for example P.Collins, "An Introduction to Regge Theory & High Energy Physics", CUP, Cambridge (1977).
12. Contribution **pa02-061** to this conference.
13. H1 Collaboration, T. Ahmed et. al. Phys. Lett. **B348** (1995) 681.
14. M. Gluck, E. Reya, A. Vogt, Z. Phys. **C53** (1992) 651-656.
15. A. Donnachie and P. Landshoff, Nucl. Phys. **B303** (1988) 634.
16. H. Jung Comp. Phys. Comm. **67** (1992) 465.
17. Contribution **pa02-063** to this conference.
18. Yu. L. Dokshitzer, JETP **46** (1977) 641.
    V. N. Gribov and L. N. Lipatov, Sov. Journ. Nucl. Phys. **15** (1972) 78.
    G. Altarelli and G. Parisi, Nucl. Phys. **B126** 1977 298.
19. P. Bruni and G. Ingelman, *Diffractive Hard Scattering at ep and $p\bar{p}$ Colliders*, DESY **93-187** (1993).
20. Contribution **pa02-060** to this conference.